Chapter 3

Corrosion Types of Magnesium Alloys

Rong-Chang Zeng, Zheng-Zheng Yin,
Xiao-Bo Chen and Dao-Kui Xu

Additional information is available at the end of the chapter

http://dx.doi.org/10.5772/intechopen.80083

Abstract

Magnesium (Mg) alloys are susceptible to corrosion in aggressive environments. Corrosion of Mg alloys depends greatly on their composition and microstructure (grain size, the size, shape and distribution of second phases), post-processing and media. In most cases, localized corrosion, such as pitting corrosion and filiform corrosion, generally occurs due to microgalvanic corrosion between the intermetallic compounds and their neighboring α-Mg matrix. However, open literature reported that several corrosion morphologies, that is, intergranular corrosion (IGC) and exfoliation corrosion (EFC), cannot appear on Mg alloys. In this chapter, all typical corrosion modes of Mg alloys and influencing factors are introduced, including general corrosion, galvanic corrosion, pitting corrosion, filiform corrosion, IGC, EFC, stress corrosion cracking (SCC), corrosion fatigue (CF) and so on. The focus is laid on pitting corrosion and EFC. Corrosion mechanisms of Mg alloys are also discussed.

Keywords: magnesium alloys, corrosion, intermetallic compounds, microstructure, biomaterials

1. Introduction

Magnesium (Mg) and its alloys can find extensive applications in transportation, 3C (computer, communication and consumer electronics) products and biomedical fields due to the lightweight, high specific strength and good biocompatibility [1, 2]. Mg alloys are susceptible to deterioration in an aggressive solution or harsh environment due to their low corrosion potential [3]. Like other metals, corrosion modes of Mg alloys can be divided into uniform or general corrosion and localized corrosion based on the phenomenon from electrochemical, composition and microstructural perspectives on macroscale. The latter predominately

includes galvanic corrosion, pitting corrosion, filiform corrosion, intergranular corrosion (IGC), exfoliation corrosion (EFC), crevice corrosion, stress corrosion cracking (SCC), corrosion fatigue (CF) and erosion corrosion. EFC and crevice corrosion, however, have been rarely reported.

Corrosion form is fundamentally influenced by metallurgical factors such as chemical composition, grain size and shapes, size, shape and distribution of secondary phases or intermetallic compound particles, inclusions, solute-aggregated grain boundaries (GBs), crystallographic orientations and dislocation density. Moreover, post-processing (i.e., extrusion and rolling) and post heat-treatment (i.e., T4, T5 and T6) exert a significant impact on corrosion mechanism. These treatments can result in evident changes in microstructure and stress. Furthermore, corrosion mode is also highly related to chlorine ion content and pH value of the corrosive solution. Localized corrosion is prone to occur under low pH value or acidic and neutral solution.

In addition, modern characterization techniques such as environmental scanning electron microscopy (ESEM), scanning electrochemical microscopy (SECM) [4] and Kelvin probe force microscopy (KPFM) [5] open a door for understanding corrosion mechanisms of Mg alloys at a microscale level.

Investigation with ESEM shows that pitting corrosion of Mg alloy AZ91 merely emerges at the sites (AlMn phases and scratches) with segregation of salt particles [6]. Application of SECM reveals that pitting corrosion of Mg is initiated from film-free region [4]. The concentration of Cl^- ions and composition of the surface film dominate the incubation and growth of active sites in film-free region. Higher concentrated chloride ions result in rapid initiation and propagation of active spots.

It is critical for design engineers to have an insight into the corrosion mechanisms and morphology of Mg alloys and to avoid sudden pre-failure of Mg parts.

2. Forms of corrosion

2.1. Uniform corrosion

Uniform corrosion can be observed on solution (T4)-treated and peak-aged WE43 alloy in 3.5 wt.% NaCl solution saturated with $Mg(OH)_2$ [7]. This scenario for the T4-treated Mg alloy relates to the formation of a protective corrosion product layer, which is composed of an inner MgO layer and an outer $Mg(OH)_2$ layer. The improvement in corrosion resistance for the aging treated alloy is ascribed to the interactions between the finely distributed precipitates and the growth of corrosion reactions.

2.2. Galvanic corrosion

Galvanic corrosion is a common corrosion feature of Mg alloys. For example, galvanic corrosion may occur when Mg parts are connected or welded with the steels in lightweight powertrains and automotive bodies. In human body fluids, severe galvanic corrosion emerges when degradable Mg screws are connected with the bone plates made of titanium and stainless steel. This scenario is attributed to Mg that is located in the most active end in galvanic

series of metals. Therefore, Mg and its alloys become the anode when connected to cathodic metals such as stainless steels and titanium alloys. This kind of galvanic corrosion is also termed bimetallic corrosion.

In some cases, galvanic corrosion occurs between two layers with different grain size in the same alloy. For instance, hot extruded Mg alloy ZK60 shows coarse grains in the outer layer and fine grains in the interior or middle layer [8]. The outer layer with a higher open corrosion potential (OCP) is passivated, while the middle layer with a lower OCP is preferentially corroded. It is the initial OCP rather than grain size that decides the initiation of galvanic corrosion [8].

At a micro-scale level, micro-galvanic corrosion may occur between the α-Mg matrix with a lower OCP and its surrounding second phases or intermetallic compounds with a higher OCP in Mg alloys. The matrix is, thus, anodic and preferentially corroded. This theory is used to explain the mechanism of localized corrosion, e.g., pitting corrosion [9], IGC [8] and EFC [5].

The nobler metals have a direct influence on the corrosion degree of the connected Mg alloys. The potential difference between Mg and other metals will be different, which can generate disparate galvanic couples and galvanic current. The galvanic current increases with the potential difference, that is, the bigger potential difference between Mg and dissimilar metal, the easier for Mg subject to corrode. The intensity of corrosion depends on the relative Volta potential differences of the micro-constituents, as well as their amounts, compositions and distributions within the alloys by KPFM [10].

The variations of pH may change the electrode reaction and polarity of galvanic metals. For instance, in an Al-Mg galvanic coupling in a neutral or weakly alkaline NaCl solution, Al acts as cathode. But with the dissolution of Mg, the solution changes into alkaline and aluminum turns into anode, which is the alkalinized effect of corrosion products of Mg alloys. Therefore, in an alkaline medium, that is, pH > 8.5, Mg alloys are basically non-corrosive. Mg alloys in acidic and neutral solutions, except for chromic acid, phosphoric acid and hydrofluoric acid that can form passive film, are susceptible to corrosion. When pH > 10.5, due to the formation of a protective $Mg(OH)_2$ film, Mg alloys have certain corrosion resistance. However, if a solution contains Cl^-, corrosion rate of Mg alloys will increase greatly.

Geometry factors such as cathode/anode area ratio, insulation distance between cathode and anode, depth of the dissolved film covering the galvanic couples and interactive mode of interaction caused by galvanic coupling can also affect the corrosion of Mg alloys.

The distance between galvanic couples is also important for corrosion behavior of Mg alloys. The distance of the galvanic current of the corrosion behavior of Mg alloys is limited. Corrosion generally occurs near the edge of such a specimen [11]. The declining amplitude decreases with the increase in the distance similarly to an exponential decay.

2.3. Pitting corrosion

Pitting corrosion is one of the most common corrosion types of Mg alloy. The generation of pits is related to chemical composition and specific microstructural features at the exposed Mg alloy surface. Chemical composition, grain size, heat treatment condition, morphology and distribution of the second phases all have an important influence on the corrosion of Mg alloys.

For sand-cast Mg alloy ZE41-T5 immersed in aggressive environment, pits initiate in the α-Mg grains neighboring T-phase (Mg_7Zn_3RE) at grain boundaries (GBs) [12]. This is attributed to galvanic corrosion, which is driven by the potential difference between the T-phase and α-Mg phase. In a subsequent immersion, the Zr-rich zones located in the center of grains become preferential corrosion sites. Small pits appear in the zones and severe attack develops.

In most cases, second phases that is, $Mg_{17}Al_{12}$ and Al_8Mn_5 are cathodic relative to α-Mg matrix [1], whereas in very limited cases, the second phases, containing rare earth (RE) and Mg in Mg alloy GW93 (Mg-Y-Gd), are more active than Mg matrix [13].

The microstructure constituents of Mg alloys are usually characterized by the α-Mg matrix and second phase or intermetallic phases, for instance, β ($Mg_{17}Al_{12}$), $MgSi_2$, AlMn(Fe), MgZn, Mg_2Zn [14], Mg_2Ca, Mg_2Sn [15], Mg_2Cu, Al_8Mn_5, I-phase (Mg_3Zn_6Y) [16] and T-phase [12]. Because in most cases, the electrode potential of these second phases is much higher than that of the α-Mg substrate, dissolution tends to emerge in the α-Mg matrix around second-phase particles. The presence of small Mg_2Ca particles coexisted with Fe and Si results in pitting corrosion of Mg-Ca alloys [17].

Occasionally, pitting corrosion is competitive when a number of second phases exist in Mg alloys. In extruded Mg alloy AZ80, there may be three kinds of intermetallic compounds: $Mg_{17}Al_{12}$, Al_8Mn_5 and Mg_2Si. Voltaic potential differences between them and the α-Mg matrix phase or contact potential difference are not the same. And corrosion preferentially occurs around AlMnFe second phase due to the fact that the potential difference between the AlMnFe phase and matrix is the biggest [18].

For Mg-Al alloys, pitting corrosion occurs along the net structure of $Mg_{17}Al_{12}$ selectively. TGC will take place in die casting Mg alloys AM50 and AM20 caused by coring. At first, corrosion pits were formed in Mn-bearing particles, then developed into corrosion cracks and extended and terminated in the high Al region or GBs of the crystals.

Pitting corrosion can be affected by grain size. Refined grains make the corrosion morphology from pitting to homogeneous or uniform corrosion.

The microstructure of an extruded Mg alloy AM60 is composed of α-Mg matrix, β phase along GBs and granular AlMn phase in grains [19]. The Al/Mn atomic ratio in AlMn phase is 1.12–1.15:1. In addition, there are a small number of Mg, Si elements and a small amount of deformation twins. The GB mainly consists of β phase. The AlMn phase is major in the grain that forms a cubic shape. There are both fine and coarse grains in the microstructure. Simultaneously, recrystallized grains form in the coarse grains. This result is due to the hot extrusion processing. The thick plate has a faster cooling rate for the outer layer and relatively slower cooling rate in the interiors, so localized recrystallization and grain abnormal growth phenomenon may occur.

In addition, pH value has a great influence on corrosion morphology of Mg alloys [19]. In acidic and neutral NaCl solutions, the α-Mg matrix phase of Mg alloy AM60 around AlMn particles is preferential to corrode. Thus, pitting corrosion of Mg alloy AM60 occurs. This may be the result of local galvanic corrosion due to a higher voltage of the AlMn phase than α-Mg matrix and β phase. In alkaline solutions, uniform corrosion of high alumina regions is observed with cellular corrosion morphology. At pH 12, the sample surface has only a few

shallow corrosion pits, which is well protected. From the morphology of the pits, the site of incipient pitting corrosion is related to the AlMn phase. The pits form on α-Mg in the area adjacent to the AlMn phase and there are many cracks in the matrix near the pits [19]. The β phase does not play a role in the corrosion process of the extruded AM60 alloy.

Figure 1 illustrates the pitting corrosion mechanism of extruded AM60 alloy. The oxide film formed on Mg alloy surface is discontinuous, which provides the adsorption sites for anions such as Cl^-. Here, the corrosion pits of Mg alloys are hemispherical. Cl^- ions are adsorbed in α phase adjacent to the AlMn particles. At the self-corrosion potential (−1.53 V/SCE), the passivation film is broken, the α phase begins to dissolve and then pitting corrosion initiates. The AlMn particle in the pits is the cathode phase, while the α-Mg phase is the anode. There are a large number of Mg^{2+} and OH^- ions in corrosion pits. When Mg^{2+} ions reach the maximum solubility, $Mg(OH)_2$ will be formed and pH value of the solution will stabilize around 10.5. Hereby, saturated Mg^{2+} ion leads to precipitation of $Mg(OH)_2$ at the bottom of the pit. And partial Mg^{2+} and OH^- ions may diffuse out of the pit with H_2 evolution, leading to the formation of $Mg(OH)_2$ precipitate outside the rim of the corrosion pit. This is the so-called occluded cell.

When an extruded Mg-1.21Li-1.12Ca-1Y alloy was immersed in Hank's solution for the first 15 min, pitting corrosion occurred at the interface of Mg_2Ca/α-Mg instead of $Mg_{24}Y_5$/α-Mg [9]. Although the potential of the Mg_2Ca particle is higher than that of the α-Mg matrix phase, the dissolution rate of Mg_2Ca particles is higher than that of α-Mg matrix phase. After subsequent immersion of 1 h, corrosion product film formed around the pitting corrosion and filiform corrosion occurred. Pitting initiation in Mg_2Ca phase α-mg matrix forms corrosion products such as $MgCO_3$, $CaCO_3$, $LiCO_3$, $Mg_3(PO_4)_2$, $Ca_3(PO_4)_2$ and Li_3PO_4 that can make the corrosion product layer denser. During the electrochemical reaction, the surface of Mg_2Ca releases OH^- and H_2 and Mg^{2+} is produced by the dissolution of α-Mg. As the reaction proceeds, $Mg(OH)_2$ precipitates on the surface of Mg_2Ca phase. Mg^{2+} reacts further with HCO_3^- or CO_3^{2-} to form $MgCO_3$ precipitates [9].

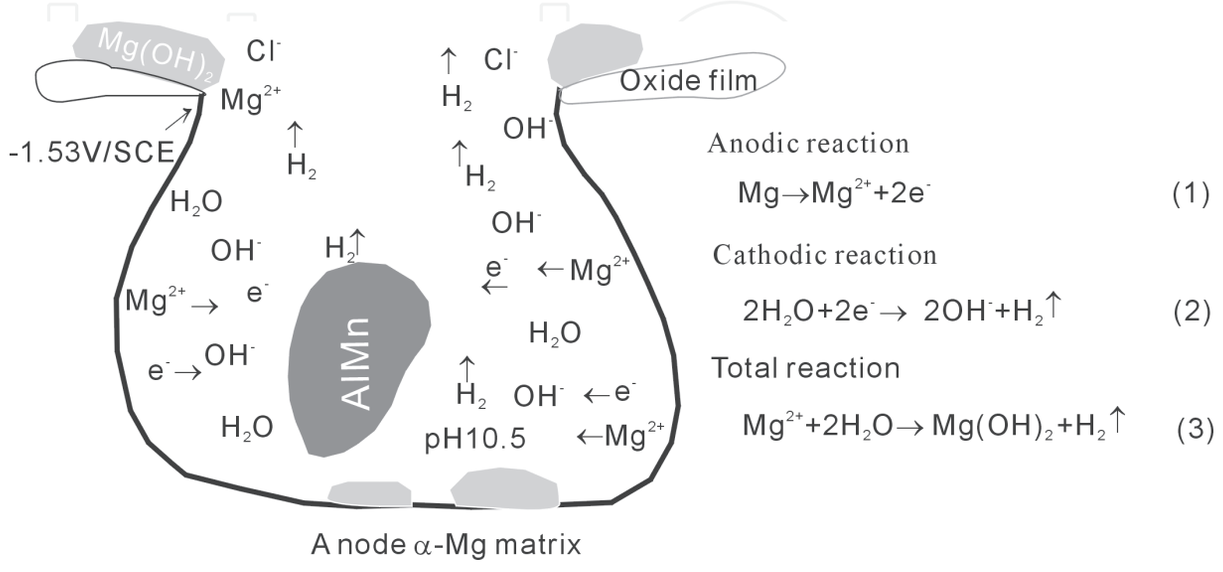

Figure 1. Model of pitting corrosion for Mg alloy AM60 [3].

The pitting corrosion occurs on as-cast dual-phase Mg-Li-Ca alloy due to the presence of Mg_2Ca particles, whereas uniform corrosion appears after an extrusion processing [20]. For the extruded Mg-Li-Ca alloy with refined microstructure, the tubular paths in the oxide film were jammed and sealed by the formation of an additional amorphous hydrated layer (**Figure 2**) and the chemical compounds, that is, LiOH, $Mg(OH)_2$, $CaCO_3$ and $MgCO_3$, the PBR values of which are between 1 and 2. In this scenario, the formation rate of the corrosion products LiOH, $Mg(OH)_2$, $CaCO_3$ $MgCO_3$ and $Ca_xMg_y(PO_4)_z$ is greater than that of the degradation rate of the Mg-Li-Ca alloy, and hence the dissolution of the alloy may be readily self-inhibited.

Pitting corrosion of Mg-Li alloys can be suppressed through grain refinement and formation of quasicrystalline or icosahedral phase (I-phase). I-phase eutectic pocket at GBs can suppress pitting corrosion and filiform corrosion of Mg-Li alloy with the presence of Zn and Y, regardless of Mg-6% Li-6% Zn-1.2% Y alloy containing a higher volume fraction of β-Li phase [16, 21].

2.4. Filiform corrosion

Filiform corrosion is also the most common type of corrosion for Mg alloys. Filiform corrosion of steel surfaces often occurs under coatings in high humidity environments. The filiform corrosion of Mg alloys is as common as pitting corrosion, but different from filiform corrosion of steels. Filiform corrosion is common on bare Mg alloy surfaces exposed to air and NaCl solution.

The pitting corrosion and filiform corrosion of Mg alloys usually occur simultaneously. Filiform corrosion originates from corrosion pits and extends forward along the active area. Corrosion of Mg alloys mainly is hydrogen evolution corrosion rather than oxygen absorption corrosion or oxygen concentration corrosion. Filiform corrosion is caused by active corrosive cells moving through the metal surface. Filiform corrosion of Mg is driven by the difference in oxygen concentration between filament head and filament tail, and thus proposed a filiform corrosion model for Mg [22]. Earlier literature reported that filiform corrosion occurs under protective coatings and anodic oxide layers, and pure Mg without coatings does not undergo filiform corrosion [1, 23].

Chloride-induced fliform corrosion of organic-coated Mg is studied by Williams *et al*. [24]. The rate of filiform corrosion advance is shown to be insensitive to the presence of oxygen, but highly dependent upon the relative humidity of the holding environment. The filiform corrosion of Mg-Li alloy produces high concentration of OH^- reacting with Mg^{2+} and Li^+ to form $Mg(OH)_2$ and LiOH, which makes filament tail alkalized, passivates and covers the corrosion products of $Mg(OH)_2$ [25]. The hydrolysis reaction acidifies the corrosion pits and becomes a filament tip. Then the tip continues to propagate forward.

2.5. Intergranular corrosion (IGC)

An earlier review [26] pointed out that IGC does not occur on Mg and its alloys. It is regarded that the attack does not enter the grain along GBs, due to the fact that GBs are almost always cathodic relative to the grain interiors. Therefore, grains are anodic with regard to GBs, and the area next to GBs will be corroded. But this is not regarded as IGC, but granular corrosion, because corrosion tends to concentrate in areas adjacent to GBs.

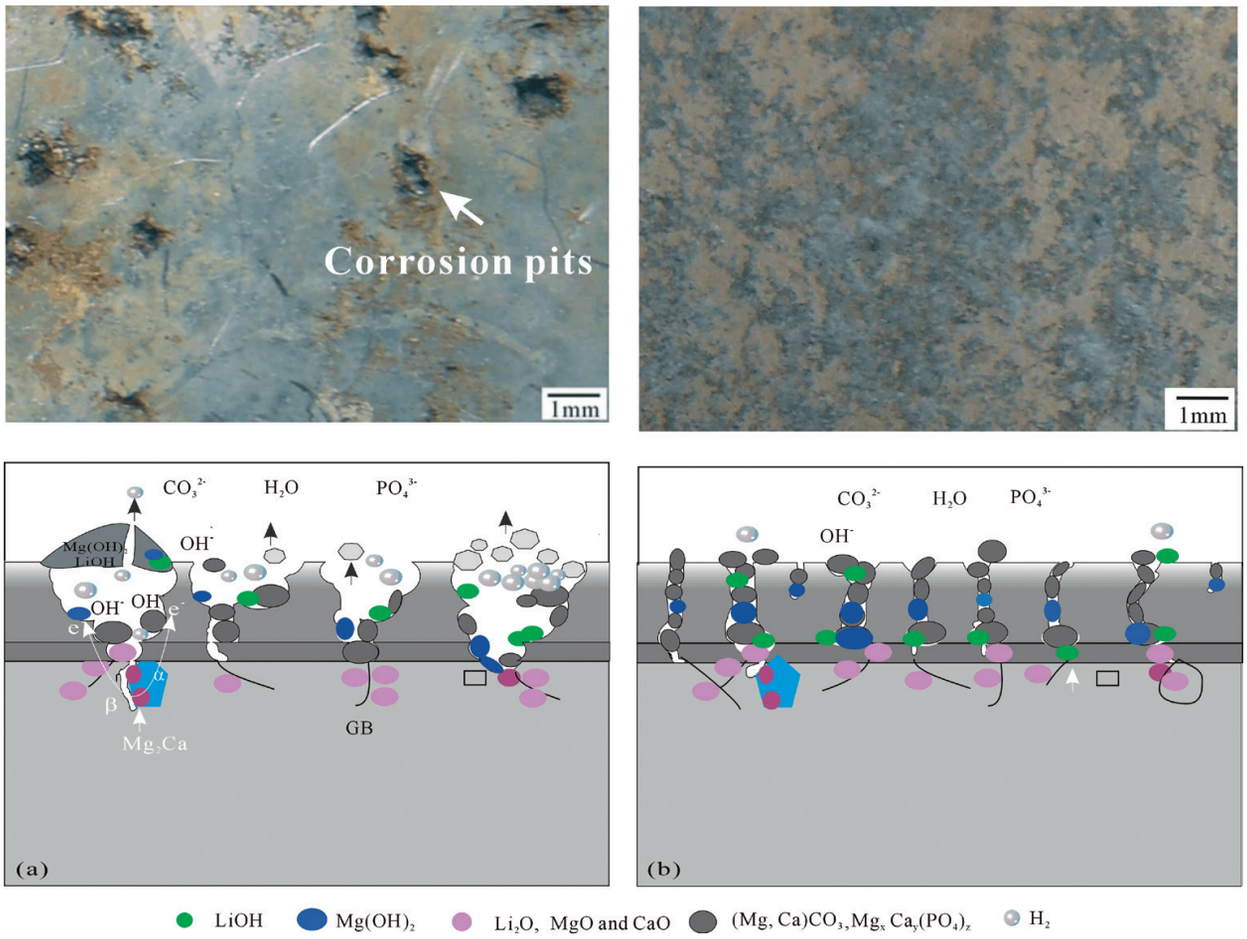

Figure 2. Schematic diagrams of the corrosion mechanisms of Mg-9Li-1Ca alloys: (a) pitting corrosion on the cast alloy and (b) tubular paths in the oxide film on the extruded alloy were jammed by corrosion products [20].

However, intergranular stress corrosion cracking (ISCC) has been observed in the process of stress corrosion of Mg alloys, which indicates that IGC of Mg alloys is truly possible. It has been found that the morphology of IGC exists in as-extruded Mg alloy AZ80 after T5 aging treatment [27]. The depth of this corrosion profile is shallow. The corrosion morphology is also due to the formation of micro-galvanic couple corrosion between $Mg_{17}Al_{12}$ and its surrounding matrix α-Mg, which is preferentially corroded [27].

From a microstructure perspective of the extrude Mg alloy ZK60, the fine second phase (Mg_2Zn) is dispersed along the GBs [8]. Thus, pearl-like corrosion pits have been observed along the GBs in the extrusion direction. For zirconium-containing aluminum-free Mg alloy ZK60, the second-phase Mg_2Zn on GBs is nobler relative to the α-Mg matrix phase, and corrosion occurs on the α-Mg matrix phase. Because zirconium is mainly distributed in the center of grains, the crystal is relatively stable. Further study discloses that the attack mainly occurs on the periphery of the grains, and no attack is seen to penetrate into the alloy along GBs. Therefore, the α-Mg matrix phase in the vicinity of GBs preferentially dissolves, which eventually leads to the whole grain peeling off. The cause of IGC is the formation of micro-galvanic corrosion between high potential finely distributed Mg_2Zn particles along the GBs and low potential matrix phase (α-Mg), which is typical IGC in Mg alloys for the first time.

2.6. Exfoliation corrosion (EFC)

EFC is usually being thought of as a special IGC. EFC on wrought Al alloys has been extensively reported [28–30]. Two essential factors exist in developing EFC: elongated grains in microstructure and different potential between the matrix and intermetallic compound precipitates at GBs [31]. However, EFC of Mg alloys has sparsely been reported. The EFC of cold-rolled Mg-14Li-1Al alloy appeared on both longitudinal and transverse surfaces [32]. At the initial stage of corrosion, oxide film formed rapidly on the surface of magnesium alloy. Then the oxide film was attacked by chlorine ions, leading to the dissolution of Mg in local areas. There corrosion micro-cracks obviously emerge along GBs, which eventually results in denudation. After annealing, the corresponding EFC disappeared. The introduction of Al suppresses the exfoliation behavior of Mg-14Li alloy. The excessive addition of Al leads to a decrease in corrosion resistance. The optimal corrosion resistance could be achieved by adding 3 wt.% Al element [33].

Recently, the corrosion morphologies of an as-extruded Mg-1Li-1Ca alloy have been investigated after immersion in 3.5 wt.% NaCl aqueous solution for 90, 120 and 150 days [5]. It is clearly that severe EFC occurs on the extruded Mg-1Li-1Ca plates (**Figure 3**) and exhibits a "lifting-up" of the surface of the samples by the force of expanding corrosion products emerging at GBs just beneath the subsurface. A large amount of corrosion debris, mainly the carbonates, for example, Li_2CO_3, $CaCO_3$ and $Mg_5(CO_3)_4(OH)_2$, can be evidently seen between the layers and on the bottom of the container.

The optical images in **Figure 4** disclose the bent outer layer and crack initiation sources and propagation directions. The cracks initiate along GBs or inside the grains, then coalescence, and arrest and propagation as well. The formation of voids or pores may be due to hydrogen blister and wedge effect resulted from the increase in volume of corrosion products.

Figure 5a demonstrates that open circuit potentials (OCPs) of the outer layer are much higher than those of the inner layer of as-extruded Mg-1Li-1Ca alloy. The gap in initial OCPs between them is greater than 88 mV/SCE. There is a risk of an increased corrosion rate for the less noble metal after galvanic coupling when the OCP difference is greater than 50 mV/SCE [8]. Macro-galvanic corrosion may, thus, occur between the inner and outer layers. **Figure 4b** shows the polarization curves of the inner zone and outer layer of the extruded Mg-1Li-1Ca alloy in 3.5 wt.% NaCl solution. Values of corrosion potential (E_{corr}) and corrosion current density (i_{corr}) were estimated through Tafel extrapolation fitting. E_{corr} values of the inner zone and outer layer are −1.639 ± 0.003 V/SCE and − 1.553 ± 0.009 V/SCE, respectively. Potential difference, $\triangle E_{corr}$ ($=E_{corr,\ outer\ layer} - E_{corr,\ inner\ zone}$ = 86 mV/SCE) of two layers is greater than 50 mV/SCE, implying the presence of galvanic corrosion.

KPFM was further used to evaluate Volta potential of the outer or skin layer and interior layer, as shown in **Figure 6**. For the interior zone, the Volta potential of extruded Mg-1Li-1Ca alloy fluctuates over a narrow range, while the skin layer in purple color corresponds to the most negative Volta potential. The Volta potential difference implies the possible presence of macro-galvanic corrosion between the interior zone and skin layer. This result is consistent with that of electrochemical tests (**Figure 5**).

http://dx.doi.org/10.5772/intechopen.80083

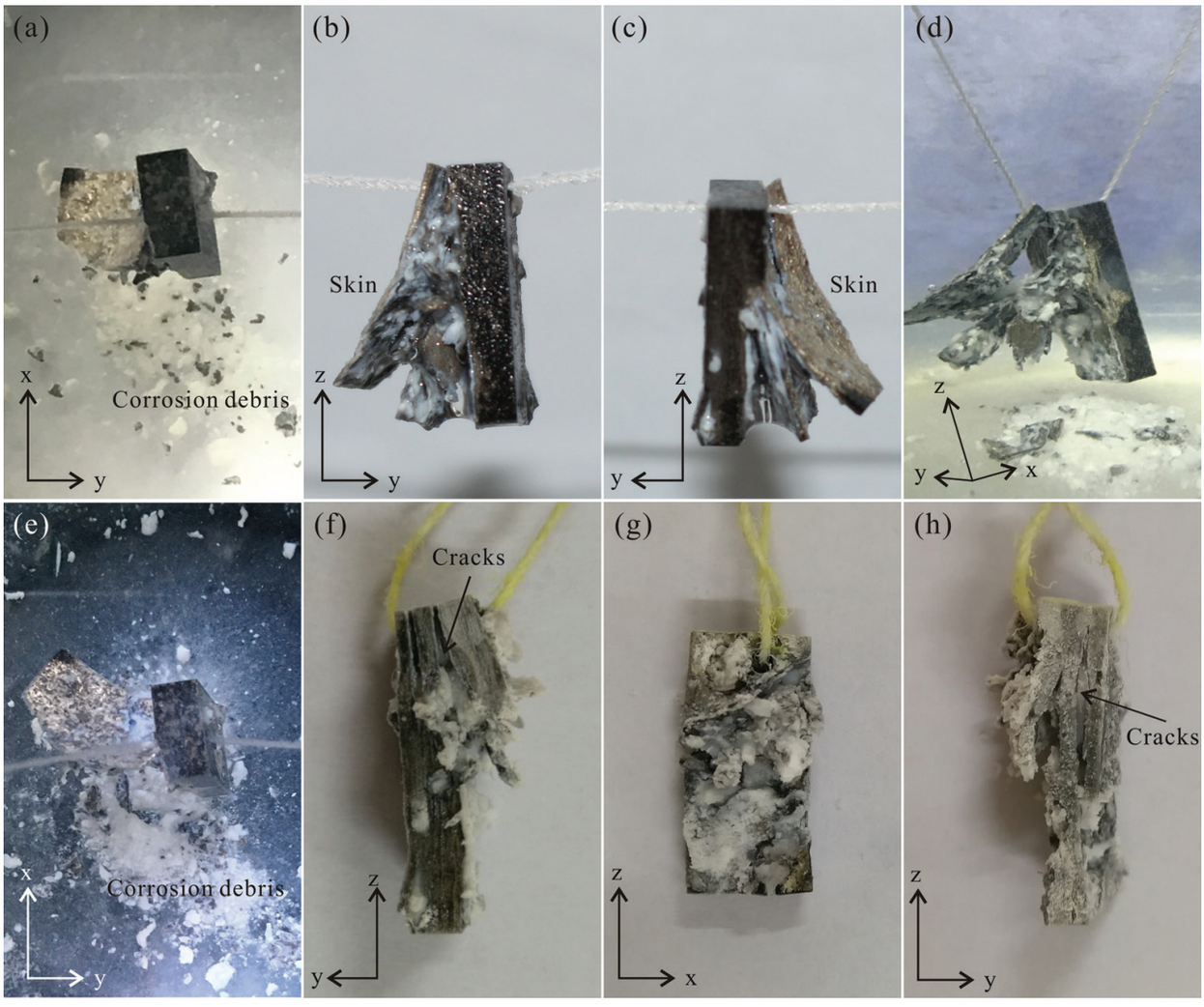

Figure 3. Corrosion macro-morphology of extruded Mg-1Li-1Ca specimens immersed in 3.5 wt.% NaCl aqueous solution after 90 days: (a)–(c); 120 days: (d) and (e); 150 days: (f)–(h) [5].

The corrosion current density, i_{corr}, for the inner layer and the outer layer of the extruded Mg-1Li-1Ca alloy is 5.789 ± 0.598 × 10^{-5} A/cm^2 and 4.718 ± 0.259 × 10^{-5} A/cm^2, respectively. Microstructure of the alloy is characterized by a fibrous structure with elongated α-Mg grains and fine intermetallic compound Mg_2Ca. The skin layer with more refined grains shows better corrosion resistance, whereas the interior with coarse grains and Mg_2Ca particles distribute along GBs and extrusion direction in a line. The inner zone exhibits a negative OCP in comparison with the skin layer. When the inner zone and outer layer are coupled together, the inner zone acts as anode and is preferentially dissolved, whereas the skin layer plays a cathodic role and is protected.

Accordingly, several factors such as microstructure (i.e., elongated microstructures and second phases) and stress dominate EFC of extruded Mg-1Li-1Ca alloy. EFC mechanisms of the extruded Mg-Li-Ca alloy are schematically illustrated in **Figure 7**. Exfoliation relates to both galvanic and wedge effects. On one hand, galvanic effect (**Figure 7a** and **b**) is resulted from the α-Mg grain and its neighboring second-phase Mg_2Ca particles, which are positioned

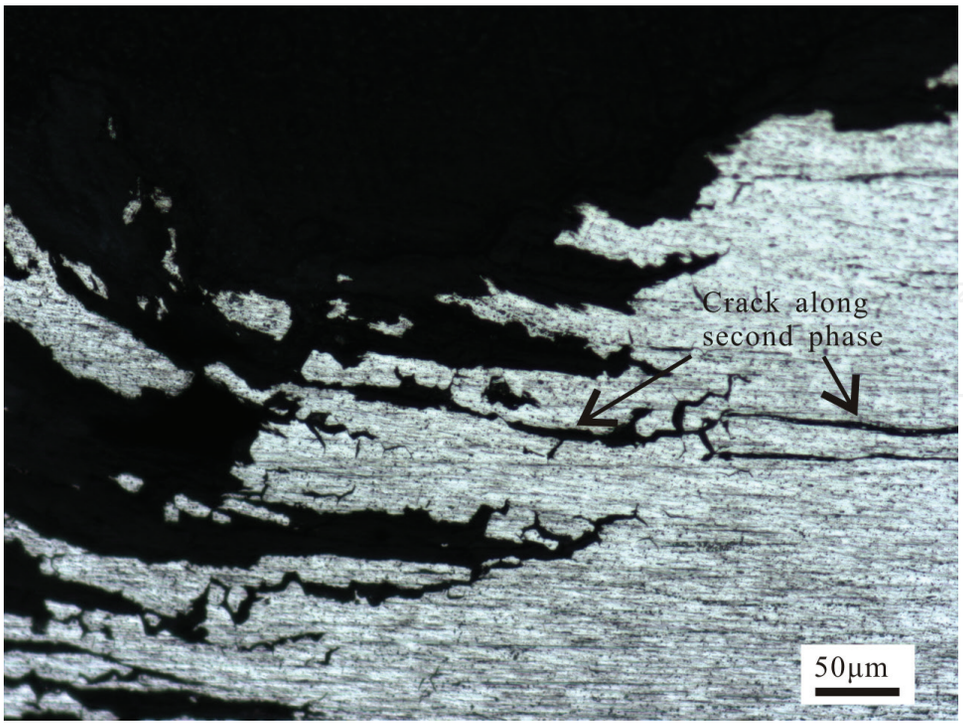

Figure 4. Optical image of cross-sectional morphologies of extruded Mg-1Li-1Ca alloy after an immersion in 3.5% NaCl aqueous solution for 21 days.

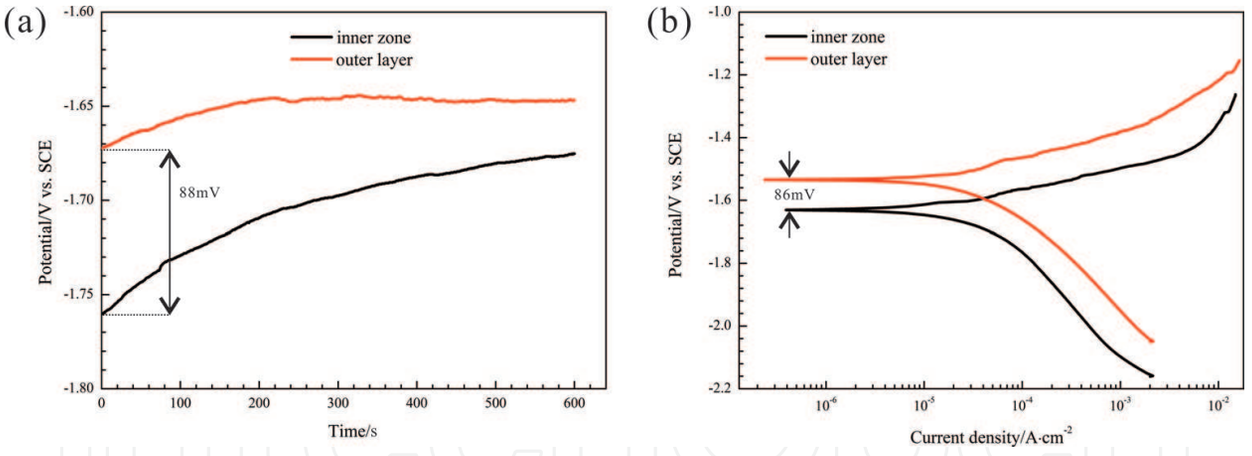

Figure 5. (a) Open circuit potential as a function of immersion time and (b) polarization curves of inner zone and outer layer of extruded Mg-1Li-1Ca alloy in 3.5 wt.% NaCl solution [5].

along the extrusion direction at both GBs and the interiors. On the other hand, the wedge effect (**Figure 7c**) is caused by the enhancement in volume of corrosion products, consisting of $Mg(OH)_2$, $Ca(OH)_2$ and carbonates such as Li_2CO_3, $CaCO_3$ and $Mg_5(CO_3)_4(OH)_2$ piled up in the cracks. Exfoliation initiates at corrosion pits and propagates along corrosion filaments (**Figure 7d**), in which filiform corrosion forms. Namely, EFC of the Mg-1Li-1Ca alloy emerged after pitting and filiform corrosion and was prone to stress corrosion. EFC of extruded Mg-Li-Ca alloys may be ascribed to a combining effect of pitting corrosion, filiform corrosion, IGC and SCC.

http://dx.doi.org/10.5772/intechopen.80083

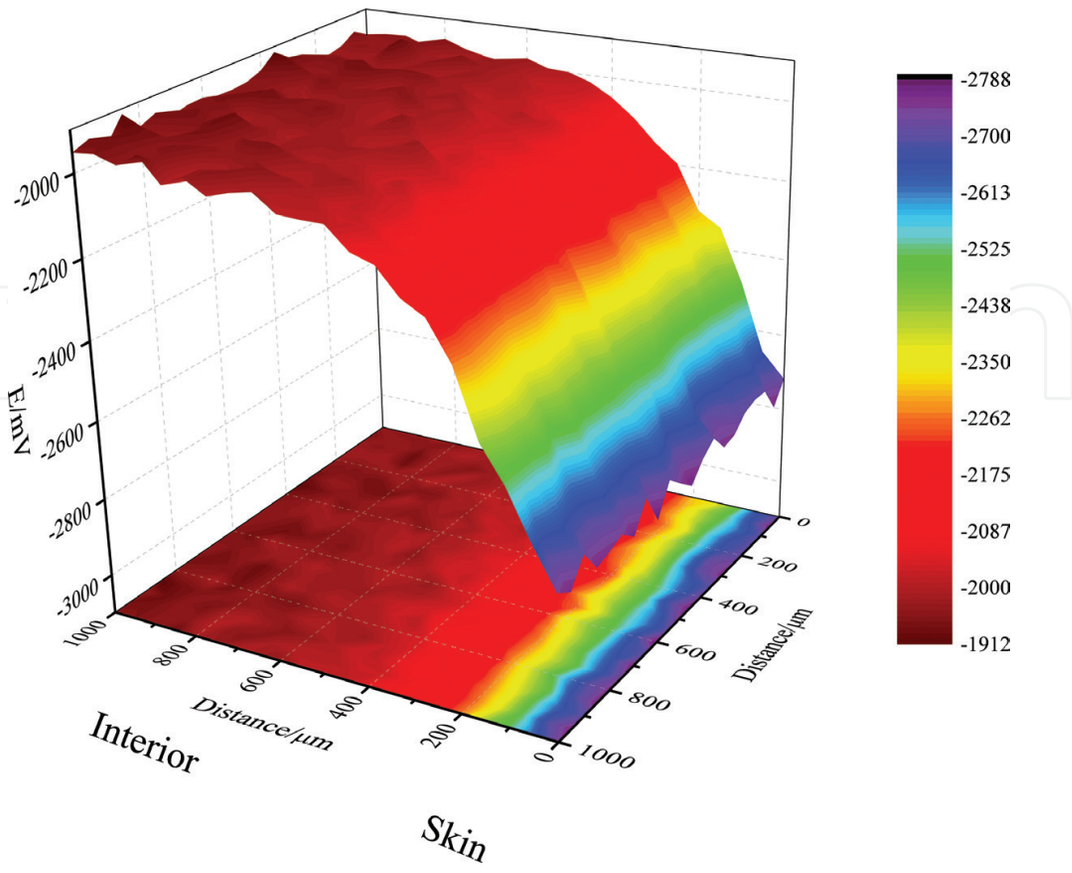

Figure 6. Surface Volta potential maps: longitudinal section of extruded Mg-1Li-1Ca alloy, detected by KPFM [5].

2.7. Crevice corrosion

Occurrence of crevice corrosion of metals, such as Fe, stainless steel and Al alloys, is generally considered to be driven by oxygen concentration (oxygen reduction cathode reaction), while for Mg alloys, the change in oxygen concentration can be neglected. Therefore, crevice corrosion of Mg alloys has been neglected before [34]. In 2011, crevice corrosion was firstly reported, which occurred in the crevice between specially treated pure Mg with unclear mechanism [35].

2.8. Stress corrosion cracking (SCC)

SCC of Mg alloys is the result of the combined action of electrochemistry and tensile mechanics. SCC can occur in any application when a stressed Mg-based component is subject to wet conditions. Basically, SCC mechanisms include anodic dissolution (AD) and hydrogen embrittlement (HE). The AD of Mg alloys is attributed to their high negative potential and the formation of a non-protective corrosion product film [36]. HE is demonstrated to widely take place due to the fact that the existence of H is inevitable. Catastrophic failure is expected when hydrogen is introduced into Mg alloys, which decreases the SCC initiation stress to below the operating stress [37]. So far, HE mechanism has not been clearly established. Pitting corrosion alleviated hydrogen into Mg alloy AZ80 and induced HE [36]. It is suggested that the cracking

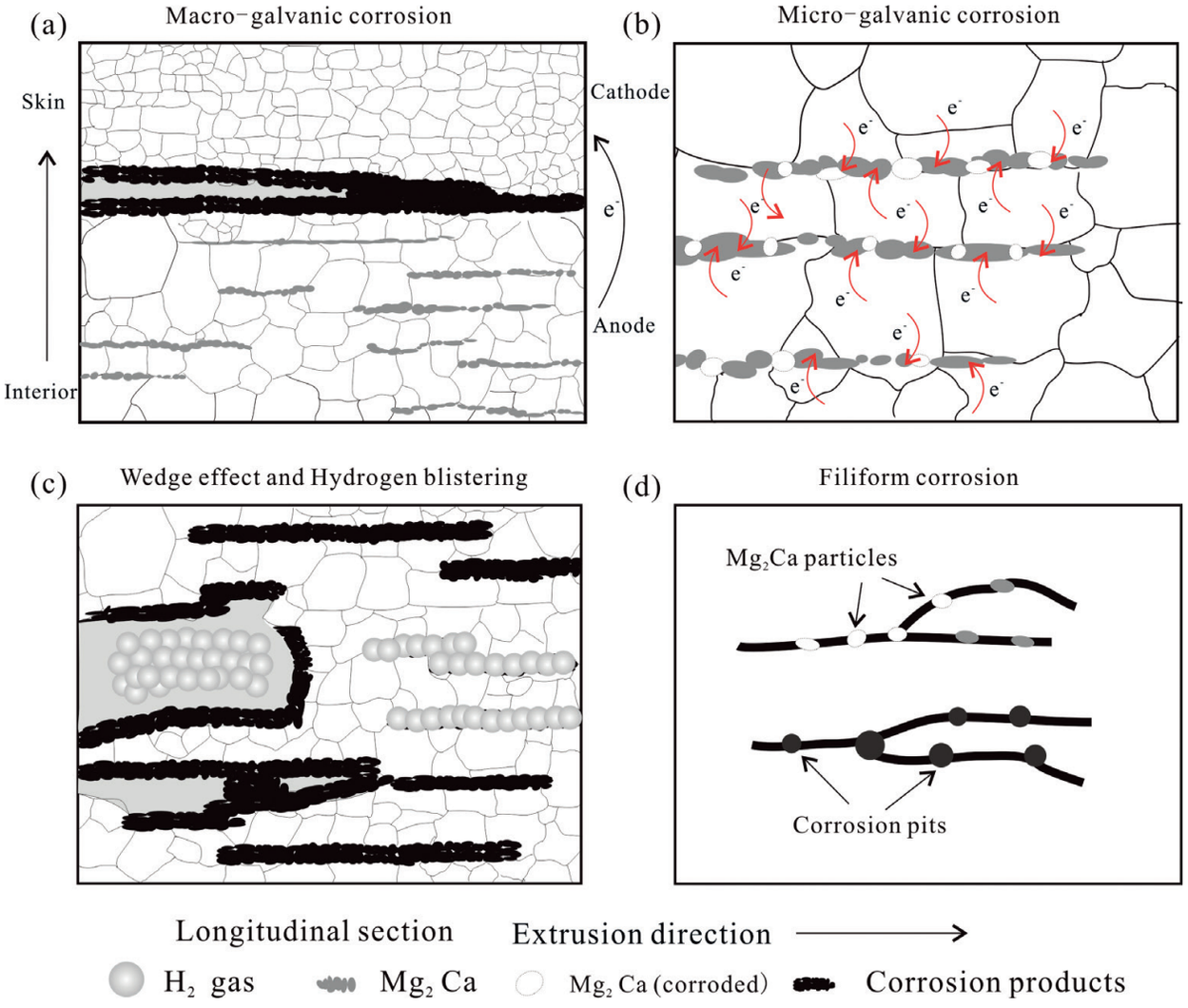

Figure 7. Schematic illustrations of EFC mechanism: (a) macro-galvanic corrosion between skin layer and interior zone, (b) micro-galvanic corrosion between Mg2Ca and α-Mg, (c) wedge effect and hydrogen blistering during EFC and (d) pitting corrosion and filiform corrosion [5].

mode of extruded Mg-7%Gd-5%Y-1%Nd-0.5%Zr (EW75) alloy is predominantly transgranular, but the partial intergranular stress corrosion cracking (IGSCC) can also be discerned at some localized area [38].

It is commonly recognized that transgranular SCC (TGSCC) of Mg alloys is a type of HE. HE models involve hydrogen-enhanced decohesion (HEDE), hydrogen-enhanced localized plasticity (HELP), adsorption-induced dislocation emission (AIDE) and delayed hydride cracking (DHC). The presence of hydride (MgH_2) phase on the fracture surface designates the DHC mechanism for a friction-stir welded magnesium alloy AZ31 [39].

One of the results of plastic deformation of polycrystalline materials with hexagonal structure is the formation of many deformation twins. Although the deformation twin plays a very important role in other fracture processes, the function on stress corrosion process is ignored. For example, at room temperature, the FCP of polycrystalline Mg alloy is related to twin [40] and GBs [41, 42]. Stress corrosion fracture surface of Mg-8.6Al alloy contains a lot of

deformation twins [43]. Twin rotation and hydrides occur during slow tensile stress corrosion of extruded Mg alloy AZ31 [39]. The relationship between SCC and deformation twin crystal plane is unclear.

Alloying elements have different impacts on SCC [43]. Al is the most important element to produce stress corrosion sensitivity of Mg alloys. Mg-Al alloys have the highest stress corrosion sensitivity, and the sensitivity increases with Al content. An Al content of Mg alloys above 0.15–2.5 wt.% will result in SCC, with the maximum concentration at 6 wt.% Al. Zn also results in SCC sensitivity of Mg alloy. The addition of zirconium or RE elements (without Al) for Mg-Zn alloys such as ZK60 and ZE10 has moderate SCC resistance. Mg-Mn alloys are the most resistant to SCC due to the absence of Al and Zn.

Mg alloys also undergo SCC in distilled water [37]. Some anions can also accelerate stress corrosion of Mg alloys. SCC sensitivity of Mg alloys in 0.1 M neutral salt solution decreases in the following order: $Na_2SO_4 > NaNO_3 > Na_2CO_3 > NaCl > CH_3COONa$.

The SCC behaviors of Mg alloy ZK60 under different conditions, that is, thin electrolyte layer (TEL) and bulk solution, had been investigated [44]. Results indicated that Mg alloy ZK60 in the bulk solution exhibits a higher SCC susceptibility with a combined SCC mechanism of weaker AD and stronger HE compared to under TEL. They further revealed that cracking mode under both conditions was dominated by TGSCC feature and related to different HE mechanisms.

The effect of bovine serum albumin (BSA) to SCC of Mg alloy AZ91D in Hanks' solution was studied in [45]. The alloy was susceptible to SCC with and without the presence of BSA. In the presence of BSA, the alloy suffered greater SCC on account of greater susceptibility to pit formation.

2.9. Corrosion fatigue (CF)

CF is a key factor determining the service life of structural metals under cyclic mechanical loads [46]. For example, car wheels must be resistant to CF. Air seems to be an aggressive atmosphere for Mg alloys. Microstructure and loading frequency have a critical influence on fatigue life and fatigue crack propagation rate (FCPR) of Mg alloys in ambient atmosphere [47–49]. Since corrosion is time-dependent, CF of Mg alloys are sensitive to loading frequency. Under 10 Hz in air, fatigue life for as-extruded Mg alloy AM60 has a certain relationship with frequency [47]. But when frequency is above 10 Hz, fatigue life is independent of frequency. This may be due to the slip or twinning of plastic deformation of Mg alloys at low frequencies and the formation of the intrusions or extrusions on the sample surface. This time seems to be enough to form an oxide film, which leads to an irreversible plastic deformation in a fatigue process. Because the plastic deformation speed is higher at a higher frequency, there's no sufficient time for extrusion of Mg alloys to react with oxygen in air to form an oxide film. Therefore, the formation of oxide film in a process of plastic deformation can be avoided at high frequency.

An investigation demonstrated the coalescence of micro-void FCP mechanism of the extruded AZ80 at a constant load amplitude fatigue test by virtue of scanning electron microscopy (SEM), transmission electron microscopy (TEM) and Auger electron spectroscopy (AES) [50].

FCPR increases with a decreasing loading frequency and an increasing load ratio. AES results designate that fatigue can markedly facilitate the fracture oxidation of magnesium alloys. In addition, the occurrence of crack closure is ascribed to plasticity instead of oxide film.

The pH value and Cl^- ion-containing solutions can significantly affect the fatigue life of Mg alloys. Fatigue life of as-extruded Mg alloy AM60 in a neutral NaCl solution was the shortest and the longest in an alkaline NaCl solution [47]. CF strength of Mg alloys AZ91HP, AZ91-T6 and AM60 in 3.5% NaCl solution decreases significantly in comparison to that in air. In addition, Cl^-, Br^-, I^- and SO_4^{2-} ions accelerate the corrosion fatigue crack growth of Mg alloys [51, 52].

Relative humidity (RH) and temperature in air have an important effect on FCP for magnesium alloys [53]. Below 60 RH%, fatigue strength is no affected. At 90 RH% and higher, however, fatigue strength is significantly reduced. The effect of RH on the fatigue strength of extruded Mg alloy AZ61 has been investigated [54]. At 55 RH%, the fatigue limitation is 145–150 MPa between 20 and 50°C. At 80 RH% fatigue fracture occurs at the stress below the fatigue limitation, which means occurrence of CF. Corrosion pits are observed on the surface and fracture initiation area of the specimens. An increase in ambient temperature from 60 to 120°C results in a higher FCPR [53].

Heat treatment (i.e., artificial aging T5) gives rise to an improvement in volume fraction of β phase, tensile strength and hardness of Mg alloy AZ80, and the fatigue life in aggressive solution at lower stress level [55].

For HCP metals, the combination of twinning and fatigue deformation with the existing twins is the main form of fatigue deformation. Dislocations and slip bands stack along the mechanical twin bands. Twins hinder the movement of dislocations, cause dislocation pile-ups, improve the internal stress of the matrix, and result in the combination of dislocation and form fatigue cracks eventually. Basically, the preferential initiation of fatigue cracks for cast Mg alloys develops at stress concentration sites such as the casting defects and pores. Fatigue cracks for wrought Mg alloys preferentially initiate at inclusions, cyclic slip bands and twin boundaries [46].

In air, fatigue crack of Mg alloy AZ80 initiates at the inclusions in the surface and subsurface [55]. Corrosion pits are often the initiation sites for CF cracks. The formation of fatigue crack in an extruded Mg alloy AM60 relates to the AlMn particles. AlMn phase is the source of fatigue crack initiation in air. When it comes to a solution medium, the corrosion fatigue crack initiates at the corrosion pits around the AlMn phase particles [56]. AD is the CF mechanism of extruded Mg alloys.

CF behavior of die-cast and extruded Mg alloys can be different. The fatigue life of die-cast and especially extruded Mg alloys AZ91D, AM50 and AZ31 is significantly decreased in 3.5% NaCl solution [57]. Extruded alloys show a higher sensitivity to 3.5% NaCl solution compared to die-cast alloys. The CF life of extruded alloys is, however, longer than that of die-cast alloys.

Fatigue behavior of Mg alloys in simulated body fluids (SBF) is similar to that in 3.5 wt.% NaCl aqueous solution. Die-cast Mg alloy AZ91D showed a fatigue limit of 50 MPa at 10^7 cycles in air in comparison to 20 MPa at 10^6 cycles in SBF at 37°C [58]. The extruded WE43 alloy

possesses a fatigue limit of 110 MPa at 10^7 cycles in air compared to 40 MPa at 10^7 cycles in SBF at 37°C. The fatigue cracks initiate at the micro-pores in air and at corrosion pits in SBF, respectively. Corrosion resistance of such two alloys decreases under cyclic loading compared to that in the static immersion test. A further study [59, 60] demonstrated that sand-cast Mg alloy AZ91D, high-purity Mg, Mg-Ca and Mg-Zn-Ca alloys are susceptible to CF in SBF. And the fatigue cracks initiate at the microstructural defects such as inclusions, cast pores, micro-cracks and corrosion pits. HE is responsible for the cracking of Mg alloy AZ91D [59].

The influence of bovine serum albumin (BSA) on CF of Mg alloys has recently been reported [61]. At stresses higher than the fatigue limit of Mg alloy AZ91D in air, mechanical factors play a predominant role. Hence, fatigue life is comparative for the alloys tested in air, Hank's solution in absence and presence of BSA. However, at lower stresses, Mg alloy AZ91D tested in Hank's solution + BSA discloses a longer fatigue life than that tested in a plain Hank's solution, indicating the inhibition impact of adsorbed BSA on corrosion and corrosion FCPR of the alloy.

Several strategies have been attempted to improve the resistance to CF. The shot-blasted Mg alloy AM60 exhibits an enhancement in fatigue strength in comparison to the die-cast one, which is ascribed to the fact that shot-blasting can induce hardening and compressive residual stress near surface region [62]. Nevertheless, coatings such as calcium phosphate and MgF_2 film can provide little improvement in CF resistance [63]. This is due to the degradation of the coating layer and existence of defects, which act as CF initiation sites under cyclical loading condition in SBF.

2.10. Erosion corrosion

Mg alloys have low surface hardness and poor resistance to wear. Wear resistance relates to load amplitude and loading frequency [64]. Wear loss of Mg alloys AZ91D and AM60B increases with normal loading force, but reduces with an increase in loading frequency. Corrosion and wear resistances can be greatly improved through micro-arc oxidation (MAO), a ceramic coating formed on the surface of Mg alloy AZ91 [65]. An $MgCO_3 \cdot 3H_2O$ film formed on Mg alloy AZ91 in HCO_3^- containing solutions is more compact and wear-resistant than porous $Mg(OH)_2$ film [66]. Further study reveals the wear diameter of Mg alloy AZ91 and its MAO coating in HCO_3^- containing solution is smaller than that in NaCl solution, indicating that the formation of corrosion products in HCO_3^- bearing solution can resist micro-abrasion to a certain extent. That is, HCO_3^- ions can promote the wear resistance of Mg alloy AZ91 with and without MAO coating. There is, however, a critical concentration of HCO_3^- for enhancement in wear resistance. During wear corrosion, oxide particles peel off from MAO coating, which is detrimental to the corrosion resistance of MAO-coated Mg alloy AZ91. Ni-P coating especially added with inorganic nano-oxide particles (i.e., TiO_2 and SiO_2) can effectively improve the wear resistance of pure Mg [40].

Flow-induced shear stress (FISS) accelerates general corrosion and localized corrosion (including pitting corrosion and erosion corrosion) due to the enhanced mass transfer and mechanical force [67]. FISS improves general corrosion rate, localized corrosion coverage ratios and

depths and removal rate of corrosion products inside the corrosion pits compared to static conditions. Flow direction has a marked influence on corrosion resistance. More severe pitting corrosion and erosion corrosion were discerned on the back ends of the Mg-Zn-Ca alloy. And the corrosion product layer facing the flow direction was delaminated from Mg alloy AZ31 stent struts.

2.11. High temperature oxidation

Since Mg and its alloys are quite active and apt to react with surrounding oxidizing media such as oxygen, nitrogen and water vapor, oxidation-resistant and mechanical properties of Mg alloys are low at elevated temperatures. The oxidation resistance of metals depends mainly on the density and coverage of surface oxide films, which are also characterized by Pilling-Bedworth ratio (PBR). PBR is related to the relative volume of oxide and its metal. When PBR is less than one, oxide film of the metal is porous and loose. When PBR is equal to or greater than one, a complete oxide film forms on the surface of the metal. Thus, the metal can be protected by such an oxide film. Basically, PBR of Mg oxide film is below one, which indicates that the oxide films of Mg alloys cannot protect substrates from the attack from the environment.

Alloying with Ca, Be and Sn as well as RE elements can improve the oxidation-resistance of Mg alloys significantly. Studies on the oxidation properties of Mg-Y-Sn, Mg-Y and Mg-Sn alloys at 500°C show that Mg-Y-Sn and Mg-Y alloys demonstrate higher oxidation resistance compared with pure Mg and Mg alloy AZ31 [68]. The formation of a compact surface oxide film on Mg-Y-Sn and Mg-Y alloys after being oxidized at 500°C for 6 h can effectively protect the alloys from further oxidation. Corrosion resistance of oxidized Mg-Y-Sn and Mg-Y alloys can be enhanced in comparison with the initial non-oxidized Mg alloys. Our recent study [5] reveals that spark of micro-arc oxidation of Mg-Li-Ca alloys initiates at the α-Mg matrix with a lower content of Ca. This is due to the ignition inhibition of Ca.

There is, however, an issue on the oxide film of Ca-containing Mg alloys. Though the value of PBR for the oxides (MgO and CaO) of Mg-Ca alloys should be less than one, they exhibit good oxidation resistance. The working mechanism related to such an unexpected performance remains unclear.

2.12. Alternative corrosion modes

In many cases, several corrosion modes are observed on the same Mg alloys simultaneously or continuously. The corrosion process of Mg-Zn-Y-Zr alloy experiences three stages: galvanic corrosion, filiform corrosion and pitting corrosion in 0.1 M NaCl solution [69]. The corrosion mechanism is governed by the second phase containing Mg, Zn and Y, which is much nobler than α-Mg matrix. There is a huge potential difference between the intermetallic compounds and their α-Mg matrix. At the first stage, the intermetallic compounds create galvanic corrosion. At the mid-stage, the intermetallic compounds prevent propagation of filiform corrosion. And at the last stage, the intermetallic compounds accelerate pitting corrosion. Different from the potential difference of Mg-Zn-Y-Zr alloy, the filaments of filiform corrosion on Mg-8Li alloy can extend a long distance due to a low potential difference between β-Li phase and α-Mg phase.

Similarly, different types of corrosion emerge alternatively for Mg-Gd-Zn alloys [70]. Galvanic corrosion appears near second phase of $(Mg, Zn)_3Gd$ in the initial immersion, and filiform corrosion emerges after an immersion of 5 h. The difference of IGC developed in 16-h immersion is ascribed to the dissolution of $(Mg, Zn)_3Gd$ phase.

As mentioned earlier [5], after a long-term immersion, the extruded Mg-Li-Ca alloys experience synergistic influence by pitting corrosion, filiform corrosion and EFC as well as SCC.

Corrosion morphology changes with the constituents of the films and volume fraction of the second phases. For Mg-7Sn alloy, the corrosion mode and rate are concerned with the quantity of the second phase Mg_2Sn and tin content of the α-Mg matrix [15]. Pitting corrosion occurs when most of tin is in the presence of Mg_2Sn phase, while filiform corrosion emerges if most of tin is solutionized in the α-Mg matrix.

3. Conclusions

Various corrosion forms of Mg alloys are introduced in this chapter. The focus is on the novel findings on EFC of extruded Mg-Li-Ca alloy. The prestigious influencing factor may be the second phases, from which the initiation of almost all the electrochemical corrosion forms of Mg alloys originates. The intrinsic corrosion of Mg alloys may be attributable to micro-galvanic corrosion between the intermetallic compounds and their neighboring α-Mg matrix. A homogenous microstructure with fine grains and intermetallic compounds can suppress the tendency of localized corrosion and lead to general corrosion. The forms of corrosion of Mg alloys may vary with extending immersion time. Several modes of corrosion may vary alternatively on the same alloy. The second phases are not always positive and act as cathode relative to α-Mg matrix. The second phases with RE may be anodic relative to α-Mg matrix.

Acknowledgements

This work is supported by National Science Foundation of China (51571134) and SDUST Research Fund (2014TDJH104).

Conflict of interest

The authors declared that they have no conflicts of interest to this work.

Appendices and nomenclature

AIDE	Adsorption-induced dislocation emission
AD	Anodic dissolution

AES	Auger electron spectroscopy
BSA	Bovine serum albumin
CF	Corrosion fatigue
DHC	Delayed hydride cracking
ESEM	Environmental scanning electron microscope
EFC	Exfoliation corrosion
FCPR	Fatigue crack propagation rate
FISS	Flow-induced shear stress
GB	Grain boundary
HE	Hydrogen embrittlement
HEDE	Hydrogen-enhanced decohesion
HELP	Hydrogen-enhanced localized plasticity
IGC	Intergranular corrosion
ISCC	Intergranular stress corrosion cracking
KPFM	Kelvin probe force microscopy
Mg	Magnesium
MAO	Micro-arc oxidation
OCP	Open corrosion potential
PBR	Pilling-Bedworth ratio
RH	Relative humidity
SEM	Scanning electron microscopy
SCC	Stress corrosion cracking
SKP	Scanning Kalvin probe
SECM	Scanning electrochemical microscopy
SBFs	Simulated body fluids
TGSCC	Transgranular SCC
TEM	Transmission electron microscopy

Author details

Rong-Chang Zeng[1]*, Zheng-Zheng Yin[1], Xiao-Bo Chen[2] and Dao-Kui Xu[3]

*Address all correspondence to: rczeng@foxmail.com

1 School of Materials Science and Engineering, Shandong University of Science and Technology, Qingdao, China

2 School of Engineering, RMIT University, Carlton, Australia

3 CAS Key Laboratory of Nuclear Materials and Safety Assessment, Institute of Metal Research, Chinese Academy of Sciences, Shenyang, China

References

[1] Zeng RC, Jin Z, Huang WJ, Dietzel W, Kainer KU, Blawert C, et al. Review of studies on corrosion of magnesium alloys. Transactions of Nonferrous Metals Society of China. 2006;**16**:763-771. DOI: 10.1016/S1003-6326(06)60297-5

[2] Zeng RC, Dietzel W, Witte F, Hort N, Blawert C. Progress and challenge for magnesium alloys as biomaterials. Advanced Engineering Materials. 2010;**10**:B3-B14. DOI: 10.1002/adem.200800035

[3] Zeng RC, Cui LY, Ke W. Biomedical magnesium alloys: Composition, microstructure and corrosion. Acta Metallurgica Sinica. 2018;**54**. DOI: 10.11900/0412.1961.2018.00032

[4] Liu W, Cao F, Xia Y, Chang L, Zhang J. Localized corrosion of magnesium alloys in NaCl solutions explored by scanning electrochemical microscopy in feedback mode. Electrochimica Acta. 2014;**132**:377-388. DOI: 10.1016/j.electacta.2014.04.044

[5] Ding Z-Y, Cui L-Y, Zeng R-C, Zhao Y-B, Guan S-K, Xu D-K, et al. Exfoliation corrosion of extruded Mg-Li-Ca alloy. Journal of Materials Science & Technology. 2018;**34**:1550-1557. DOI:10.1016/j.jmst.2018.05.014

[6] Chen J, Wang J, Han E-H, Ke W. In situ observation of pit initiation of passivated AZ91 magnesium alloy. Corrosion Science. 2009;**51**:477-484. DOI: 10.1016/j.corsci.2008.11.024

[7] Chu P-W, Marquis EA. Linking the microstructure of a heat-treated WE43 Mg alloy with its corrosion behavior. Corrosion Science. 2015;**101**:94-104. DOI: 10.1016/j.corsci.2015.09.005

[8] Zeng R, Kainer KU, Blawert C, Dietzel W. Corrosion of an extruded magnesium alloy ZK60 component—The role of microstructural features. Journal of Alloys & Compounds. 2011;**509**:4462-4469. DOI: 10.1016/j.jallcom.2011.01.116

[9] Zeng RC, Qi WC, Zhang F, Cui HZ, Zheng YF. In vitro corrosion of Mg–1.21Li–1.12Ca–1Y alloy. Progress in Natural Science: Materials International. 2014;**24**:492-499. DOI: 10.1016/j.pnsc.2014.08.005

[10] Coy AE, Viejo F, Skeldon P, Thompson GE. Susceptibility of rare-earth-magnesium alloys to micro-galvanic corrosion. Corrosion Science. 2010;**52**:3896-3906. DOI: 10.1016/j.corsci.2010.08.006

[11] Jia J, Atrens A, Song G, Muster TH. Simulation of galvanic corrosion of magnesium coupled to a steel fastener in NaCl solution. Materials & Corrosion. 2015;**56**:468-474. DOI: 10.1002/maco.200403855

[12] Neil WC, Forsyth M, Howlett PC, Hutchinson CR, Hinton BRW. Corrosion of magnesium alloy ZE41—The role of microstructural features. Corrosion Science. 2009;**51**:387-394. DOI: 10.1016/j.corsci.2008.11.005

[13] Song YW, Shan DY, Han EH. Pitting corrosion of a rare earth Mg alloy GW93. Journal of Materials Science & Technology. 2017;**33**:954-960. DOI: 10.1016/j.jmst.2017.01.014

[14] Zeng RC, Wang L, Zhang DF, Cui HZ, Han EH. In vitro corrosion of Mg-6Zn-1Mn-4Sn-1.5Nd/0.5Y alloys. Frontiers of Materials Science. 2014;**8**:230-243. DOI: 10.1007/s11706-014-0256-6

[15] Liu XB, Shan DY, Song YW, Chen RS, Han EH. Influences of the quantity of Mg2Sn phase on the corrosion behavior of Mg–7Sn magnesium alloy. Electrochimica Acta. 2011;**56**:2582-2590. DOI: 10.1016/j.electacta.2010.12.030

[16] Xu DK, Han EH. Effect of quasicrystalline phase on improving the corrosion resistance of a duplex structured Mg–Li alloy. Scripta Materialia. 2014;**71**:21-24. DOI: 10.1016/j.scriptamat.2013.09.025

[17] Zeng R-C, Qi W-C, Cui H-Z, Zhang F, Li S-Q, Han E-H. In vitro corrosion of as-extruded Mg–Ca alloys—The influence of Ca concentration. Corrosion Science. 2015;**96**:23-31. DOI: 10.1016/j.corsci.2015.03.018

[18] Andreatta F, Apachitei I, Kodentsov AA, Dzwonczyk J, Duszczyk J. Volta potential of second phase particles in extruded AZ80 magnesium alloy. Electrochimica Acta. 2006;**51**:3551-3557. DOI: 10.1016/j.electacta.2005.10.010

[19] Zeng RC, Zhou WQ, Han EH, Ke W. Effect of pH values onas-extruded magnesium alloy AM60. Acta Metallurgica Sinica. 2005;**41**:307-311. DOI: 10.3321/j.issn:0412-1961.2005.03.017

[20] Zeng R-C, Sun L, Zheng Y-F, Cui H-Z, Han E-H. Corrosion and characterisation of dual phase Mg–Li–Ca alloy in Hank's solution: The influence of microstructural features. Corrosion Science. 2014;**79**:69-82. DOI: 10.1016/j.corsci.2013.10.028

[21] Xu DK, Han EH. Effects of icosahedral phase formation on the microstructure and mechanical improvement of Mg alloys: A review. Progress in Natural Science: Materials International. 2012;**22**:364-385. DOI: 10.1016/j.pnsc.2012.09.005

[22] Evans UR, Kruger J, Brown BF. Localized corrosion. In: Proceedings of the NACE International Corrosion Conference Series (NACE-3); 6-10 December 1971; Williamsburg, Virginia: NACE; 1974. p. 1215-1235

[23] Ghali E, editors. General, Galvanic, and Localized Corrosion of Aluminum and Its Alloys. Chichester: John Wiley & Sons, Inc.; 2010. 176-214 pp. DOI: 10.1002/9780470531778.ch5

[24] Williams G, Grace R. Chloride-induced filiform corrosion of organic-coated magnesium. Electrochimica Acta. 2011;**56**:1894-1903. DOI: 10.1016/j.electacta.2010.09.005

[25] Song YW, Shan DY, Chen RS, Han EH. Corrosion characterization of Mg–8Li alloy in NaCl solution. Corrosion Science. 2009;**51**:1087-1094. DOI: 10.1016/j.corsci.2009.03.011

[26] Song GL, Atrens A. Corrosion mechanisms of magnesium alloys. Advanced Engineering Materials. 1999;**1**:11-33. DOI: 10.1002/(SICI)1527-2648(199909)1:1<11::AID-ADEM11>3.0.CO;2-N

[27] Zeng R, Han E, Wei KE. Corrosion of artificial aged magnesium alloy AZ80 in 3.5 wt pct NaCl Solutions. Journal of Materials Science & Technology. 2007;**23**:353-358

[28] Reboul MC, Bouvaist J. Exfoliation corrosion mechanisms in the 7020 aluminium alloy. Materials & Corrosion. 1979;**30**:700-712. DOI: 10.1002/maco.19790301006

[29] Robinson MJ. Mathematical modelling of exfoliation corrosion in high strength aluminium alloys. Corrosion Science. 1982;**22**:775-790. DOI: 10.1016/0010-938X(82)90013-0

[30] Conde A, Damborenea JD. Electrochemical modelling of exfoliation corrosion behaviour of 8090 alloy. Electrochimica Acta. 1998;**43**:849-860. DOI: 10.1016/S0013-4686(97)00218-1

[31] Marlaud T, Malki B, Henon C, Deschamps A, Baroux B. Relationship between alloy composition, microstructure and exfoliation corrosion in Al–Zn–Mg–Cu alloys. Corrosion Science. 2011;**53**:3139-3149. DOI: 10.1016/j.corsci.2011.05.057

[32] Morishige T, Doi H, Goto T, Nakamura E, Takenaka T. Exfoliation corrosion behavior of cold-rolled Mg-14 mass% Li-1 mass% Al alloy in NaCl solution. Materials Transactions. 2013;**54**:1863-1866. DOI: 10.2320/matertrans.MAW201301

[33] Morishige T, Obata Y, Goto T, Fukagawa T, Nakamura E, Takenaka T. Effect of Al composition on the corrosion resistance of Mg-14 mass% Li system alloy. Materials Transactions. 2016;**57**:1853-1856. DOI: 10.2320/matertrans.M2016247

[34] Atrens A, Liu M, Abidin NIZ. Corrosion mechanism applicable to biodegradable magnesium implants. Materials Science & Engineering B. 2011;**176**(20):1609-1636. DOI: 10.1016/j.mseb.2010.12.017

[35] Shi ZM, Atrens A. An innovative specimen configuration for the study of Mg corrosion. Corrosion Science. 2011;**53**:226-246. DOI: 10.1016/j.corsci.2010.09.016

[36] Bobby Kannan M, Dietzel W. Pitting-induced hydrogen embrittlement of magnesium–aluminium alloy. Materials & Design. 2012;**42**:321-326. DOI: 10.1016/j.matdes.2012.06.007

[37] Atrens A, Winzer N, Dietzel W. Stress corrosion cracking of magnesium alloys. Advanced Engineering Materials. 2011;**13**:11-18. DOI: 10.1002/adem.200900287

[38] Wang SD, Xu DK, Han EH, Dong C. Stress corrosion cracking susceptibility of a high strength Mg-7%Gd-5%Y-1%Nd-0.5%Zr alloy. Journal of Magnesium & Alloys. 2014;**2**:335-341. DOI: 10.1016/j.jma.2014.11.004

[39] Zeng RC, Dietzel W, Zettler R, Gan WM, Sun XX. Microstructural evolution and delayed hydride cracking of FSW-AZ31 magnesium alloy during SSRT. Transactions of Nonferrous Metals Society of China. 2014;**24**:3060-3069. DOI: 10.1016/S1003-6326(14)63443-9

[40] Calderón JA, Jiménez JP, Zuleta AA. Improvement of the erosion-corrosion resistance of magnesium by electroless Ni-P/Ni(OH)2-ceramic nanoparticle composite coatings. Surface and Coatings Technology. 2016;**304**:167-178. DOI: 10.1016/j.surfcoat.2016.04.063

[41] Partridge PG. Cyclic twinning in fatigued close-packed hexagonal metals. Philosophical Magazine. 1965;**12**:1043-1054. DOI: 10.1080/14786436508228133

[42] Makar GL, Kruger J, Sieradzki K. Stress corrosion cracking of rapidly solidified magnesium-aluminum alloys. Corrosion Science. 1993;**34**:1311-1323. DOI: 10.1016/0010-938X(93)90090-4

[43] Zeng RC. Corrosion and corrosion fatigue in deformed magnesium alloys [doctoral thesis]. Institute of Metal Research, Chinese Academy of Sciences; 2003 (in Chinese)

[44] Zhou LF, Liu ZY, Wu W, Li XG, Du CW, Jiang B. Stress corrosion cracking behavior of ZK60 magnesium alloy under different conditions. International Journal of Hydrogen Energy. 2017;**42**:26162-26174. DOI: 10.1016/j.ijhydene.2017.08.161

[45] Harandi SE, Banerjee PC, Easton CD, Singh Raman RK. Influence of bovine serum albumin in Hanks' solution on the corrosion and stress corrosion cracking of a magnesium alloy. Materials Science & Engineering C Materials for Biological Applications. 2017;**80**:335-345. DOI: 10.1016/j.msec.2017.06.002

[46] Wang BJ, Wang SD, Xu DK, Han EH. Recent progress in fatigue behavior of Mg alloys in air and aqueous media: A review. Journal of Materials Science & Technology. 2017;**33**:1075-1086. DOI: 10.1016/j.jmst.2017.07.017

[47] Zeng RC, Han EH, Liu L, Xu YB, Ke W. Effect of rolled microstructure on fatigue properties of magnesium alloy AM60. Chinese Journal of Materials Research. 2003;**17**:241-246. DOI: 10.3321/j.issn:1005-3093.2003.03.004

[48] Zeng RC, Han EH, Ke W. Fatigue and corrosion fatigue of magnesium alloys. Materials Science Forum. 2005;**488**:721-724. DOI: 10.4028/www.scientific.net/MSF.488-489.721

[49] Zeng RC, Ke W, Han EH. Influence of load frequency and ageing heat treatment on fatigue crack propagation rate of as-extruded AZ61 alloy. International Journal of Fatigue. 2009;**31**:463-467. DOI: 10.1016/j.ijfatigue.2008.07.005

[50] Zeng RC, Xu YB, Ke W, Han EH. Fatigue crack propagation behavior of an as-extruded magnesium alloy AZ80. Materials Science & Engineering A. 2009;**509**:1-7. DOI: 10.1016/j.msea.2009.01.013

[51] Potzies C, Ulrich KK. Fatigue of magnesium alloys. Advanced Engineering Materials. 2004;**6**:281-289. DOI: 10.1002/adem.200400021

[52] Ogarevic VV, Stephens RI. Fatigue of magnesium alloys. Annual Review of Materials Research. 2003;**20**:141-177. DOI: 10.1146/annurev.ms.20.080190.001041

[53] Zeng RC, Ke W, Han EH. Effect of temperature and relative humidity on fatigue crack propagation behavior of AZ61 magnesium alloy. Materials Science Forum. 2007;**546-549**: 409-412. DOI: 10.4028/www.scientific.net/MSF.546-549.409

[54] Sajuri ZB, Miyashita Y, Mutoh Y. Fatigue characteristics of an extruded AZ61 magnesium alloy. Journal of Japan Institute of Light Metals. 2002;**52**:161-166. DOI: 10.2464/jilm.52.161

[55] Zeng RC. Mechanism of corrosion fatigue for as-extruded magnesium alloy AZ80. Chinese Journal of Materials Research. 2004;**18**:561-567. DOI: 1005-3093(2004)06-0561-07 (in Chinese)

[56] Zeng RC, Ke W. Corrosion fatigue of as-extruded AM60 magnesium alloy. Chinese Journal of Materials Research. 2005;**19**:1-7. DOI: 10.3321/j.issn:1005-3093.2005.01.001 (in Chinese)

[57] Eliezer A, Gutman EM, Abramov E, Unigovski Y. Corrosion fatigue of die-cast and extruded magnesium alloys. Journal of Light Metals. 2001;**1**:179-186. DOI: 10.1016/S1471-5317(01)00011-6

[58] Gu XN, Zhou WR, Zheng YF, Cheng Y, Wei SC, Zhong SP, et al. Corrosion fatigue behaviors of two biomedical Mg alloys—AZ91D and WE43—In simulated body fluid. Acta Biomaterialia. 2010;**6**:4605-4613. DOI: 10.1016/j.actbio.2010.07.026

[59] Jafari S, Singh Raman RK, Davies CHJ. Corrosion fatigue of a magnesium alloy in modified simulated body fluid. Engineering Fracture Mechanics. 2015;**137**:2-11. DOI: 10.1016/j.engfracmech.2014.07.007

[60] Bian D, Zhou WR, Liu Y, Li N, Zheng YF, Sun ZL. Fatigue behaviors of HP-Mg, Mg–Ca and Mg–Zn–Ca biodegradable metals in air and simulated body fluid. Acta Biomaterialia. 2016;**41**:351-360. DOI: 10.1016/j.actbio.2016.05.031

[61] Harandi SE, Raman RKS. Corrosion fatigue of a magnesium alloy under appropriate human physiological conditions for bio-implant applications. Engineering Fracture Mechanics. 2017;**186**:134-142. DOI: 10.1016/j.engfracmech.2017.09.031

[62] Khan SA, Bhuiyan MS, Miyashita Y, Mutoh Y, Koike T. Corrosion fatigue behavior of die-cast and shot-blasted AM60 magnesium alloy. Materials Science & Engineering A. 2011;**528**:1961-1966. DOI: 10.1016/j.msea.2010.11.033

[63] Jafari S, Singh Raman RK. In-vitro biodegradation and corrosion-assisted cracking of a coated magnesium alloy in modified-simulated body fluid. Materials Science & Engineering C. 2017;**78**:278. DOI: 10.1016/j.msec.2017.04.079

[64] Huang WJ, Hou B, Pang YX, Zhou ZR. Fretting wear behavior of AZ91D and AM60B magnesium alloys. Wear. 2006;**260**:1173-1178. DOI: 10.1016/j.wear.2005.07.023

[65] Zhang XP, Zhao ZP, Wu FM, Wang YL, Wu J. Corrosion and wear resistance of AZ91D magnesium alloy with and without microarc oxidation coating in Hank's solution. Journal of Materials Science. 2007;**42**:8523-8528. DOI: 10.1007/s10853-007-1738-z

[66] Chen J, Zeng R-C, Huang W-J, Zheng Z-Q, Wang Z-L, Wang J. Characterization and wear resistance of macro-arc oxidation coating on magnesium alloy AZ91 in simulated body fluids. Transactions of Nonferrous Metals Society of China. 2008;**18**:s361-s364. DOI: 10.1016/S1003-6326(10)60232-4

[67] Wang J, Giridharan V, Shanov V, Xu Z, Collins B, White L, et al. Flow-induced corrosion behavior of absorbable magnesium-based stents. Acta Biomaterialia. 2014;**10**:5213-5223. DOI: 10.1016/j.actbio.2014.08.034

[68] Yu XW, Jiang B, Yang H, Yang QS, Xia XS, Pan FS. High temperature oxidation behavior of Mg-Y-Sn, Mg-Y, Mg-Sn alloys and its effect on corrosion property. Applied Surface Science. 2015;**353**:1013-1022. DOI: 10.1016/j.apsusc.2015.07.011

[69] Song YW, Shan DY, Chen RS, Han E-H. Effect of second phases on the corrosion behaviour of wrought Mg–Zn–Y–Zr alloy. Corrosion Science. 2010;**52**:1830-1837. DOI: 10.1016/j.corsci.2010.02.017

[70] Srinivasan A, Huang Y, Mendis CL, Blawert C, Kainer KU, Hort N. Investigations on microstructures, mechanical and corrosion properties of Mg–Gd–Zn alloys. Materials Science & Engineering A. 2014;**595**:224-234. DOI: 10.1016/j.msea.2013.12.016